JGP Journal of General Physiology

COMMUNICATION

KCa1.1 channels contribute to optogenetically driven post-stimulation silencing in cerebellar molecular layer interneurons

Merouann Kassa[1], Jonathan Bradley[2], Abdelali Jalil[1], and Isabel Llano[1]

Using cell-attached recordings from molecular layer interneurons (MLI) of the cerebellar cortex of adult mice expressing channel rhodopsin 2, we show that wide-field optical activation induces an increase in firing rate during illumination and a firing pause when the illumination ends (post-stimulation silencing; PSS). Significant spike rate changes with respect to basal firing rate were observed for optical activations lasting 200 ms and 1 s as well as for 1 s long trains of 10 ms pulses at 50 Hz. For all conditions, the net effect of optical activation on the integrated spike rate is significantly reduced because of PSS. Three lines of evidence indicate that this PSS is due to intrinsic factors. Firstly, PSS is induced when the optical stimulation is restricted to a single MLI using a 405-nm laser delivering a diffraction-limited spot at the focal plane. Secondly, PSS is not affected by block of GABA-A or GABA-B receptors, ruling out synaptic interactions amongst MLIs. Thirdly, PSS is mimicked in whole-cell recording experiments by step depolarizations under current clamp. Activation of Ca-dependent K channels during the spike trains appears as a likely candidate to underlie PSS. Using immunocytochemistry, we find that one such channel type, KCa1.1, is present in the somato-dendritic and axonal compartments of MLIs. In cell-attached recordings, charybdotoxin and iberiotoxin significantly reduce the optically induced PSS, while TRAM-34 does not affect it, suggesting that KCa1.1 channels, but not KCa3.1 channels, contribute to PSS.

Introduction

In the last decade, the use of optogenetic techniques to target neurons in specific cerebellar regions has greatly advanced the understanding of neuronal connectivity within and between cerebellar structures. Notably, various studies have identified regions and specific neuronal subtypes that contribute both to sensory-motor processing and to various cognitive aspects of cerebellar function (Deverett et al., 2019; Gao et al., 2016; Heiney et al., 2014; Kimpo et al., 2014; Lee et al., 2015; Nguyen-Vu et al., 2013; Prestori et al., 2020; Sarnaik and Raman, 2018). New pathways for the transfer of information between the cerebellar cortex and other brain areas have also been identified with the aid of optogenetic tools, with their contribution to reward-oriented behavior by the cerebellum being put forward recently (Carta et al., 2019). Most of these studies have relied on channel rhodopsin 2 (ChR2), a protein which contains a light-gated cation channel that fluxes monovalent cations as well as calcium ions. Although ChR2 is generally used as an excitatory-opsin, there is indeed evidence that activation of this opsin can lead to an excitation–inhibition sequence (in Purkinje cells: Lee et al., 2015). The underlying mechanism behind this observation, however, has been largely neglected and remains unexplored.

In the present work we investigate the effect of optical activation of ChR2 in molecular layer interneurons (MLIs) of the cerebellar cortex in adult mice by performing non-invasive spike recordings in loose-cell attached mode. We show that ChR2 elicits, as expected, an increase in firing rate upon illumination. This is, in turn, followed by a pause in firing as soon as illumination is terminated. We find that this pause is cell intrinsic, i.e., not due to synaptic interactions in the MLI network, and that the activation of KCa1.1 channels in the stimulated cell likely contributes to this behavior.

Materials and methods

Experimental procedures followed animal care guidelines of the University Paris Descartes and were approved by the Prefecture de Police (#A-750607) in agreement with the European Directive 86/609/EEC and by the ethical committee of the University Paris Descartes.

[1]Université Paris Cité, Centre National de la Recherche Scientifique, Saints-Pères Paris Institute for the Neurosciences, Paris, France; [2]Institut de Biologie de l'Ecole Normale Superieure (IBENS), Ecole Normale Superieure, Centre National de la Recherche Scientifique, INSERM, Paris Sciences et Lettres Research University, Paris, France.

Electrophysiology and optogenetics

Experiments were performed in slices prepared from nNOS-ChR2 BAC mice ranging from P32 to P72. These mice express the light-activated protein channel rhodopsin 2 (ChR2-EYFP) specifically in MLIs (Kim et al., 2014; Zhao et al., 2011). Slices were prepared in ice-cold protective solution (Zhao et al., 2011) containing, in mM, 93 N-methyl-D-glucamine, 2.5 KCl, 1.25 NaH_2PO_4, 25 $NaHCO_3$, 0.5 $CaCl_2$, 10 $MgCl_2$, 20 HEPES, 5 Na ascorbate, 2 thiourea, 3 Na pyruvate, and 25 glucose (HCl added to bring pH to 7.4). Slice maintenance was at 34°C in standard recording saline (BBS, in mM: 125 NaCl, 2.5 KCl, 1.25 NaH_2PO_4, 25 $NaHCO_3$, 2 $CaCl_2$, 1 $MgCl_2$, and 10 glucose) until transferred to the set-up, where BBS was perfused at a rate of 2 ml/min at 34°C.

In order to ascertain ChR2-EYFP expression, two photon imagings of the molecular layer were performed at an excitation wavelength of 910 nm. Previous work has shown that the least invasive method of recording MLI firing is to use a loose-seal configuration under voltage clamp (Alcami et al., 2012). Accordingly, most results from this study were based on this method. Loose-seal recordings were obtained from MLI somata with pipettes filled with HEPES-buffered extracellular saline (in mM: 150 NaCl, 2.5 KCl, 1 $MgCl_2$, 2 $CaCl_2$, and 10 HEPES, adjusted to a pH of 7.3 with 1 M NaOH solution). Pipette resistance was 5–8 MΩ and seal resistances ranged from 24 to 200 MΩ. No voltage was applied to the patch pipette. To photostimulate the ChR2 protein, most experiments used single-photon widefield LED stimulation. The output of a 470 nm LED (OptoFlash; Cairn Research) was coupled to a 1-mm optic fiber positioned inside the slice chamber and light pulses of 0.2 or 1 s duration as well as 1-s-long trains of 10 ms pulses at 50 Hz were applied at 1 min intervals (4 mW out of the fiber). In a subset of experiments, focal activation was achieved using a laser (Obis 405 nm laser, Coherent), coupled to the side port of the microscope by an optical fiber (0.4–1 mW out of the objective). Excitation had a full width at half-maximum of ∼350 nm laterally and of 8.6 µm in the z-axis, as detailed in Gomez et al. (2020). To test drugs, a control period of 3–6 runs was first recorded, and the agent was added thereafter to the perfusion saline only if the spike rate was stable. Analysis during the drug period commenced 3–5 min after drug perfusion and included 3–6 runs. The GABA-A blocker SR95531 hydrobromide, the GABA-B blocker CGP55845 hydrochloride, iberiotoxin, charybdotoxin, and TRAM-34 were purchased from Hello Bio.

For current clamp experiments, the tight-seal whole-cell recording configuration was used with a pipette solution containing, in mM, 140 K Gluconate, 5.4 KCl, 4.1 $MgCl_2$, 10 HEPES-K, 0.4 Na-GTP, 4 Na-ATP, and 1 mM EGTA-K. Voltages were acquired using the fast mode of an EPC-10 HEKA amplifier and corrected off-line for a −10 mV junction potential. Currents ranging from 1 to 20 pA were injected to maintain a basal firing rate between 2.5 and 7.3 Hz. The current pulse amplitude was adjusted to increase firing rate to levels similar to those observed with ChR2 optical activation, values ranging from 10 to 30 pA.

Spike analysis was performed in the Igor Pro environment (Wavemetrics) using the Spike detection option of Neuromatic software (Rothman and Silver, 2018). Average firing rates were calculated for the period prior to stimulation, during the stimulation and during the 1 s following the end of the stimulation. Peri-stimulus time histograms (PSTH) were produced with a bin width of 100 ms. Integration was done with the same bin width. To analyze the temporal evolution of spikes from cell-attached recording (Fig. 7 and related text), individual spike traces were generated, values for the peak amplitudes of the positive and negative components were calculated and normalized to the pre-stimulation values.

Statistical parameters are reported as mean ± SEM. Statistical tests were performed using two-tailed Wilcoxon signed rank test. Groups were considered significantly different for $P \leq 0.05$. The test details are reported in the text.

Immunostaining and confocal imaging

KCa1.1 channel expression was examined either in nNOS-ChR2 BAC (N = 3; PN 50) or in wild-type mice virally expressing GCaMP3 in MLIs. To obtain GCaMP3 expression, C57BL6 mice (N = 3; PN 33) of either sex were deeply anesthetized, mounted on an stereotaxic frame, and the cerebellar vermis was injected with 1.0 µl of a solution containing AAV2/1.hSyn.Flex.GCaMP3.WPRE.SV40 (Addgene, 7e12 GC/ml) and AAV1.cKit::Cre.bGHpA (0.17e12 GC/ml; Villette et al., 2019). Injection procedures were as detailed previously (Astorga et al., 2015; Astorga et al., 2017) and mice were used 3 wk after injection. Mice were prepared for sectioning by systemic paraformaldehyde perfusion (4% in PBS), 50-µm-thick sagittal cerebellar slices were cut and immunostaining was carried out as described recently (Gomez et al., 2020).

To stain for KCa1.1 channels, the primary mouse monoclonal antibody Slo1, clone L6/60 (Millipore) was used at a dilution of 1:100. A chicken polyclonal GFP antibody (1:1,000 dilution; Invitrogen) was used to enhance the visualization of MLIs in GCaMP3-expressing slices. Secondary antibodies were goat anti-chicken A488 (1:1,000 dilution; Abcam) and goat anti-mouse A546 (1:1,000 dilution; Invitrogen). Confocal images were acquired on a Zeiss LSM710 confocal microscope, as described in Gomez et al. (2020). Analysis of confocal stacks was carried out using the ImageJ-NIH software.

Results

In order to assess the effects of optical activation of ChR2, we monitored spike rate with loose-seal cell-attached recording from MLI somata in sagittal slices of adult nNOS-ChR2 BAC mice, which express ChR2 specifically in MLIs (Zhao et al., 2011; Kim et al., 2014). As shown in Fig. 1 A1, when 1-s-long light pulses were delivered to the slice through an optic fiber, the firing rate evolved in a temporal sequence of excitation–inhibition. As expected, during the light pulse, the firing rate increased and remained elevated for the duration of the optical excitation. Upon light termination, spike activity abruptly stopped during more than 1 s, before returning slowly to baseline values, a phenomenon hereon called post-stimulation silencing (PSS). This temporal sequence was elicited reproducibly upon repeated light pulses and yielded a robust biphasic time course in the PSTH (black histogram in Fig. 1 A2). On average, firing rates increased from basal values of 7.55 ± 1.07 Hz to 41.16

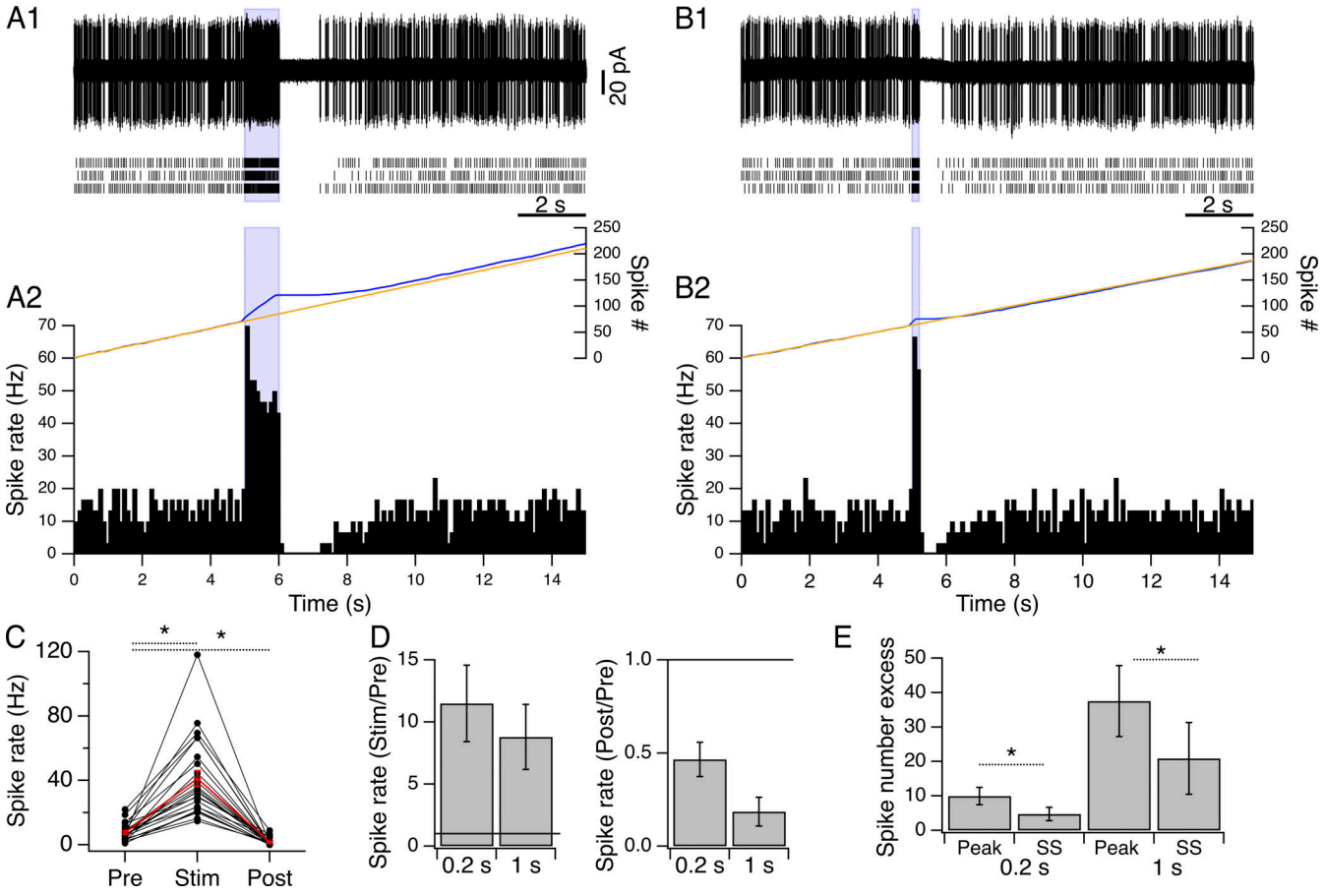

Figure 1. **Excitation–inhibition sequence during optical MLI activation. (A1)** Upper trace: Loose-seal cell-attached recording from an MLI soma. Lower traces: Raster plots for three consecutive runs at 1 min intervals. Spike rate increases during the 1-s-long light pulse (purple rectangle). After the light pulse there is a period with no spike activity. **(A2)** Black: PSTH for the three runs. The blue trace, with corresponding y axis on the right, displays the integral of the PSTH. The yellow line is an extrapolation of a linear fit of the blue trace during the pre-stimulus period, where blue and yellow traces superimpose. The distance between blue and yellow traces, representing spike number excess, increases during the light pulse and decreases thereafter. **(B1 and B2)** Same experiment, but using a 200 ms light pulse, which results in a similar increase in spike rate and a shorter post-stimulus silent period. **(C)** The biphasic effect of optical stimulation on spike rate was observed for 24 MLIs tested with 1-s-long light pulses. Pre denotes the average spike rate during the period preceding the pulse, Stim corresponds to the spike rate averaged over the 1-s-long pulse, and Post denotes the spike rate during the 1 s subsequent to the light pulse. Wilcoxon paired test P < 1.2e7 for both changes. **(D)** Pooled data on a subset of experiments in which 200 ms and 1-s-long optical stimulations were performed (three to seven repetitions per cell, alternating durations). Significant increases in the spike rate are observed during the light pulse for both durations (left) as well as a significant decrease in the spike rate compared to pre-stimulus values during the post-stimulation period (right). **(E)** Spike number excess is significantly larger at the end of the light pulse (labeled "peak") compared to steady state (SS), both for 0.2 s long pulses (Wilcoxon paired test P = 0.01) and for 1 s long pulses (Wilcoxon paired test P = 0.004).

± 4.91 Hz during the 1-s light pulse and fell to 1.58 ± 0.48 Hz during the 1 s period after illumination (N = 24; both changes are significant with Wilcoxon paired test P < 1.2e7; Fig. 1 C). As illustrated in Fig. 1 B, we found a similar excitation–inhibition sequence elicited by 200-ms light pulses. Pooled data from a subset of recordings (N = 9) in which 200 ms and 1-s-long light pulses were alternated are shown in Fig. 1, D and E. Spike rate changes with respect to baseline values are significant at the two light pulse durations, both for the excitation phase and for the ensuing period of silence, with ratios of the firing rate during the stimulation to pre-stimulation values equal to 11.5 ± 3.1 and 8.8 ± 2.6 for the 200 ms and 1 s pulses, respectively (Wilcoxon paired test P = 0.04 in both cases), and ratios for post- versus pre-stimulation periods equal to 0.46 ± 0.09 and 0.18 ± 0.08 for the 200 ms and 1 s pulses, respectively (P = 0.04 in both cases).

The blue traces in Fig. 1, A2 and B2 are the integral of the PSTH, whereas the yellow lines represent the number of spikes predicted if the basal firing rate had remained steady during the recordings. The difference between blue and yellow traces is the excess in spike number elicited by optical stimulation. This difference reached a maximum at the end of optical stimulation, and it decreased thereafter to a new steady-state value due to PSS. The extent of compensation associated with PSS varied among cells. It was almost complete in the representative experiment as shown in Fig. 1, A and B, as the steady-state blue minus yellow difference was slightly positive after 1 s stimuli (Fig. 1 A2), and slightly negative after 0.2 s stimuli (Fig. 1 B2). When quantified the results indicate a significant reduction of the spike increase at steady state compared to that at the peak for both the assayed light durations (Fig. 1 E). On average, the

spike number excess was reduced from 10.6 ± 2.3 to 4.7 ± 1.9 following a 0.2-s-long light pulse, and from 37.5 ± 10.3 to 20.8 ± 10.4 following a 1-s-long light pulse, representing roughly a halving of the spike increase in each case (Wilcoxon paired tests: P = 0.01 for 200 ms and 0.004 for 1 s; *N* = 9). Taken together, we found that PSS greatly reduced the net effect of light stimuli on integrated spike numbers.

Because trains of light pulses are often used during optogenetic studies, we compared the effect of 10-ms-long light pulses delivered at 50 Hz during 1 s with the 1-s-long pulse protocol of Fig. 1 A. As illustrated in Fig. 2, A and B, both protocols induced both significant increases in spike frequency during stimulation and significant spike pauses with ratios of the firing rate during the stimulation to pre-stimulation values of 5.7 ± 1.2 for 50 Hz trains and 6.5 ± 1.5 for continuous pulse (Wilcoxon paired test P = 0.03 in both cases; *N* = 6) and ratios for post- versus pre-stimulation periods of 0.29 ± 0.13 for trains and 0.28 ± 0.11 for continuous pulse (P = 0.04 in both cases; *N* = 6). While the results obtained with either stimulation protocol were variable among experiments, they displayed a very close correlation between the two protocols. This applied both to the spike rate increase during light activation (Fig. 2 C) as well as to the post-activation pause (Fig. 2 D) indicating that PSS proceeds similarly following trains of light stimulations or following sustained pulses of light stimulation. The similarity between the two protocols is not surprising in view of the relatively slow kinetics of ChR2 activation (time to peak in the order of 10 ms, desensitization time constant of 25 ms according to Mattis et al. [2011]); since these results were obtained at 22°C, approximately twofold faster kinetics may be expected in our experiments at 36°C because of the temperature sensitivity of ChR2 kinetics (Chater et al., 2010).

Because the experiments above did not spatially restrict the light beam, a large fraction of the MLI network was stimulated. One potential consequence of this could be activation of MLI-MLI synapses and release of spill-over GABA (activating either GABA-A and/or GABA-B receptors in the recorded MLI). To address whether the biphasic time course of ChR2 responses observed in MLIs resulted from extrinsic or intrinsic factors, we restricted the optical activation area using a 405-nm laser delivering a diffraction-limited spot at the focal plane (Trigo et al., 2009). Laser stimulation still elicited a sequence of excitation–inhibition, as illustrated in Fig. 3 A. In six MLIs, 200-ms laser pulses increased the spike rate by a factor of 7.9 ± 2.2, not significantly different to that reported above with widefield illumination (Fig. 3 B; P = 0.32 for Wilcoxon unpaired test). This excitation was followed by a silencing period, with a ratio of post-stimulation to basal rates of 0.48 ± 0.1, not significantly different from that obtained with widefield illumination (Fig. 3 C; P = 0.54 for Wilcoxon unpaired test). These results suggest that the extent of PSS does not depend on the illumination area and, therefore, that an intrinsic mechanism is at play. To further test this hypothesis, we next blocked GABA receptors. As illustrated by the examples in Fig. 4, neither the block of GABA-A receptors (Fig. 4 A) nor the block of GABA-B receptors (Fig. 4 B) significantly affected the silencing effect. Pooled data show no difference for the spike ratio during the post-stimulus period over control for both groups of experiments (Fig. 4 C; P values for Wilcoxon paired tests are 0.62 for the SR vs. control group and 1 for the CGP vs. control group; *N* = 5 in both cases).

The lack of effects of GABA-A and GABA-B receptor antagonists suggests that an intrinsic membrane property underlies the spike silencing. The question then arises as to whether ChR2-induced silencing can be mimicked by direct stimulation of the recorded MLI. To this effect, whole-cell current-clamp recordings were performed, and the holding current adjusted such that the MLI displayed a basal spike rate in the range of rates observed in loose cell-attached recording (between 2.5 and 7.3 Hz). To simulate the optical activation, 1-s-long current steps were delivered at intervals of 1 min (Fig. 5, A1 and A3). On average, firing rates increased from basal values of 4.4 ± 1.1 to 57.8 ± 8.6 Hz during the 1-s pulse and fell to 0.8 ± 0.5 Hz in the 1-s period after the pulse (*N* = 5; Fig. 5 C). Mean respective ratios were 16.6 ± 4.5 and 0.2 ± 0.1 (Fig. 5 D); both changes are significant with P values for Wilcoxon paired test for Pre vs. Stim of 0.03, for Pre vs. Post of 0.03 (*N* = 5). These results indicate that direct depolarization, like ChR2-induced depolarization, leads to a significant inhibition after the stimulus.

To compare further the effects of optogenetic stimulation versus direct current injection, we examined the values of the action potential (AP) peak and of the after-hyperpolarization potential (AHP) during the two protocols. The AHP minimum was shifted in the depolarizing direction both during current injection (by 3.2 ± 0.4 mV; Fig. 5 A2, lower panel) and during optogenetic stimulation (by 2.6 ± 0.6 mV; Fig. 5 B2, lower panel). By contrast, the peak AP amplitude was little affected during current injection (shift of −1.1 ± 0.5 mV; Fig. 5 A2, upper panel) or by optogenetic stimulation (0.0 ± 1.3 mV; Fig. 5 B2, upper panel; *N* = 3 experiments with both types of stimulation). These results are in line with previous data showing that optogenetic stimulation in MLIs produces inward currents displaying little adaptation (Kim et al., 2014).

In a wide range of mammalian neurons, prolonged depolarization elicits a compensatory spike inhibition due to activation of voltage-gated calcium channels and consequent activation of calcium-dependent potassium channels including KCa1.1 channels (for review, see Faber and Sah, 2003). Such a scenario appears plausible here because MLIs contain a large complement of somatic KCa1.1 channels (Chavas et al., 2004) and effects of KCa1.1 blockers on GABA release have indicated that these channels are also present in axonal terminals (Tan and Llano, 1999). The impact of these channels on AP patterns depends on their subcellular localization (Bock and Stuart, 2016). To assess KCa1.1 expression in MLIs, we performed immunostaining of mice cerebellar slices using the Slo1 antibody and, as reported previously (Misonou et al., 2006), staining was observed in the Purkinje cell (PC) layer as well as in the molecular layer (Fig. 6 A). Due to the dense staining from the neuropil in the molecular layer, we were not able to distinguish the MLI signal from that of the PC arborization. To improve the spatial resolution, we resorted to viral-mediated sparse labeling of MLIs by injecting high titer of a GCaMP3 encoding adeno-associated virus (AAV) and limiting titer of a cre encoding AAV driven by the cKit promoter (Villette et al., 2019), and performed the

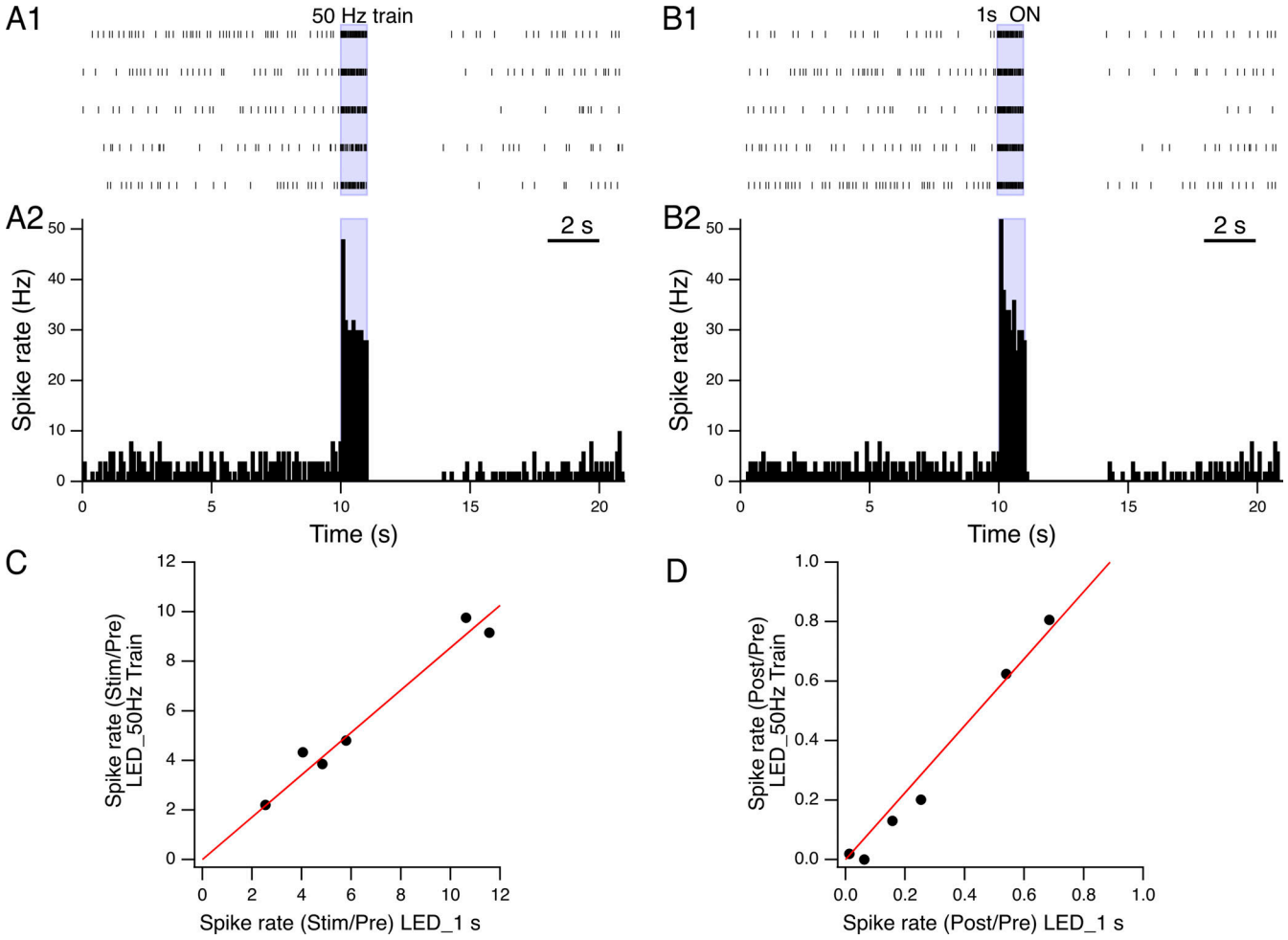

Figure 2. **Train of optostimulations induces PSS. (A1)** Raster plots for the spike activity recorded from an MLI during a 1-s-long train of 10 ms light pulses delivered at 50 Hz. **(A2)** Corresponding PSTH. **(B1 and B2)** Raster plots and PSTH from the same recording during 1-s-long light pulses. **(C)** Pooled data (N = 6) on the ratio of spike rate during the stimulation to basal rates, using either continuous light pulse or a 50 Hz train lasting 1 s. The red line shows a fit of the data by a linear function constrained to passing through the origin, with a slope of 0.85. **(D)** From the same group of cells, pooled data on the ratio of post-stimulation to basal rates. Slope of linear fit, 1.12.

immunostaining on slices from these mice (see Materials and methods). Because of the sparseness of the GCaMP3 protein expression, only a few MLIs are labeled, and their neurites can be followed with excellent resolution when using an antibody to GFP (green channel in Fig. 6 B). Extraction of the MLI KCa1.1 signal, performed by applying a binary mask from the GFP signal to the Slo1 staining, reveals KCa1.1 localized in the soma as well as in the dendritic and axonal compartments, including the axon initial segment of the MLIs (Fig. 6, C and D) with evidence for channel clustering throughout the axonal arborization (Fig. 6, E and F). These results suggest that KCa1.1 channels are indeed poised to contribute to electrical signaling by MLIs.

We tested this hypothesis by analyzing the effect of charybdotoxin (ChTx) during optogenetic stimulation. As illustrated in Fig. 7, A1 and A2, the toxin induced changes in both amplitude and shape of the extracellularly recorded spike. Although basal firing rates were not significantly affected by addition of ChTx (8.53 ± 39 Hz in control, 9.31 ± 2.02 Hz in toxin; Wilcoxon paired test P = 0.3, N = 6), the shape of AP traces obtained in cell-attached recordings was changed by ChTx (Fig. 7 A2). As discussed in an earlier work, such traces reflect the derivative of the intracellularly recorded AP time course, and the positive and negative phases of the cell-attached traces reflect the slopes of AP ascending and descending phases, respectively (Alcami et al., 2012). In control conditions, both positive and negative components of the spikes were rapid, indicating very rapid underlying AP kinetics (Fig. 7 A2 a). Optogenetic stimulation did not alter this signal (example in Fig. 7 A2, b and c, group analysis in Fig. 7 B). These results are consistent with the lack of effect of optogenetic stimulation on the peak of the AP observed in whole-cell recording results (Fig. 5). In both cases, the results suggest a simple mode of light stimulation, similar to that of a steady depolarizing current injection. In ChTx, the amplitude of the positive component of the spike signal in cell-attached recordings was similar to control (mean ChTx/control amplitude ratio: 1.04 ± 0.08, P = 0.84, Wilcoxon paired test, N = 6; Fig. 7 B). By contrast, the amplitude of the second component was markedly smaller in ChTx than in control (example in Fig. 7

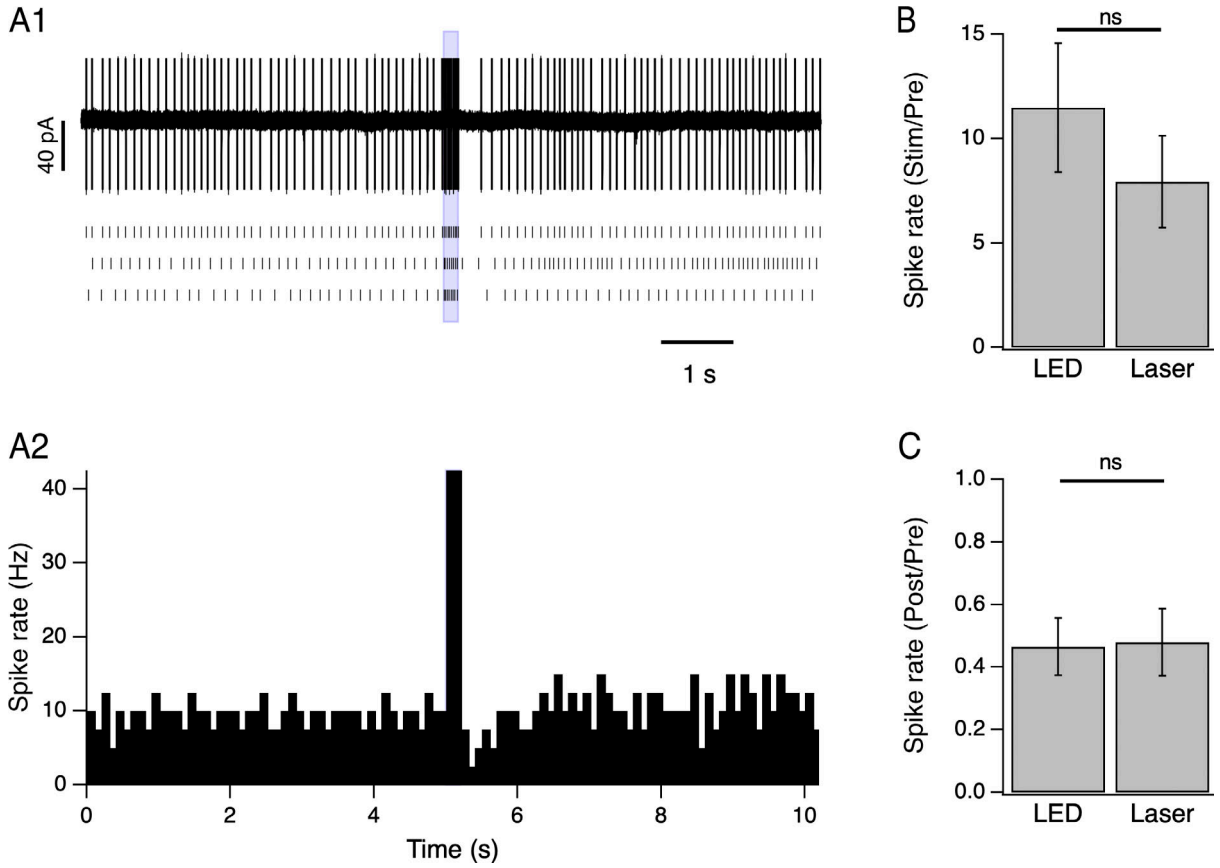

Figure 3. **Local optical stimulation induces PSS. (A1)** Upper trace: Loose-seal cell-attached recording from an MLI soma. Lower traces: Raster plots for three consecutive runs of 200 ms long light pulses confined to the recorded MLI using a 405 nm laser. **(A2)** PSTH for the three runs. **(B)** Pooled data on the ratio of spike rate during the stimulation to basal rates obtained with 200-ms-long LED-based light pulses (same data pool as in Fig. 1 D) and 200 ms 405 nm laser-based light pulses (N = 6). **(C)** Pooled data on the ratio of post-stimulation to basal rates obtained with 200-ms-long LED-based light pulses (same data pool as in Fig. 1 D) and 200 ms 405 nm laser-based light pulses (N = 6).

A2 d, and group analysis in Fig. 7 B; mean ChTx/control amplitude ratio: 0.29 ± 0.05, P = 0.03, Wilcoxon paired test, N = 6). This indicated that ChTx does not alter the upstroke of the underlying AP but that it slows down the AP recovery phase. The results therefore suggest that in control conditions, ChTx-sensitive channels are phasically activated by each spike, resulting in a shortening of spike duration. These ChTx-sensitive channels are likely KCa1.1 channels, as further discussed below. The results of Fig. 7 are consistent with previous reports that KCa1.1 channels shorten the duration of the spike waveform in various brain regions (Faber and Sah, 2003; Gu et al., 2007; Niday and Bean, 2021; Storm, 1987; Womack et al., 2004). In spite of the effect of ChTx on spike waveform, however, the firing rate increase that was directly associated with opto-stimulation was similar in the absence or presence of toxin (P = 0.31 for Wilcoxon paired test; N = 6). These results are in line with previous observations in other neuronal types indicating that KCa1.1 blockage results in a strong effect on AP shape yet weakly affects basal or immediate depolarization-driven firing (Gu et al., 2007; Womack et al., 2009). Nevertheless, we found ChTx drastically reduced the silencing effect following light stimulation (P = 0.03 for Wilcoxon paired test; N = 6; pooled data in Fig. 7 C and exemplar time course of the effect of ChTx in Fig. 7 A3).

Because ChTx can act on KCa3.1 channels as well as on KCa1.1 channels (Hermann and Erxleben, 1987), we examined the silencing effect following light stimulation in the presence of iberiotoxin (IbTx) which targets specifically KCa1.1 channels (Candia et al., 1992) and of TRAM-34, previously used in cerebellar slices to assess the role of KCa 3.1 channels (Engbers et al., 2012). Similar to ChTx, IbTx did not alter the amplitude of the first spike component (mean IbTX/control amplitude ratio: 1.13 ± 0.16, P = 0.44, Wilcoxon paired test; N = 6), and it reduced the amplitude of the second spike component (mean IbTx/control amplitude ratio: 0.22 ± 0.04, P = 0.03, Wilcoxon paired test, N = 6). IbTx also mimicked the effects of ChTx on spike silencing, resulting in a significant reduction of PSS (with ratios for post-versus pre-stimulation periods of 0.11 ± 0.04 in control and 0.37 ± 0.03 in toxin; P = 0.03 for Wilcoxon paired test; N = 6) without significant effects on the spike rate increase during photostimulation (with ratios for stimulation versus pre-stimulation periods of 10.4 ± 3.8 in control and 4.0 ± 0.30 in toxin; P = 0.09 for Wilcoxon paired test; N = 6). On the other hand, TRAM-34 affected neither the spike rate increase nor the pause following optical stimulations (P = 0.81 and 0.62, respectively, for Wilcoxon paired test; N = 5). Pooled results from these experiments (Fig. 7 C) are in accord with a role of KCa1.1 channels in the silencing effect observed after activation of ChR2 in MLIs.

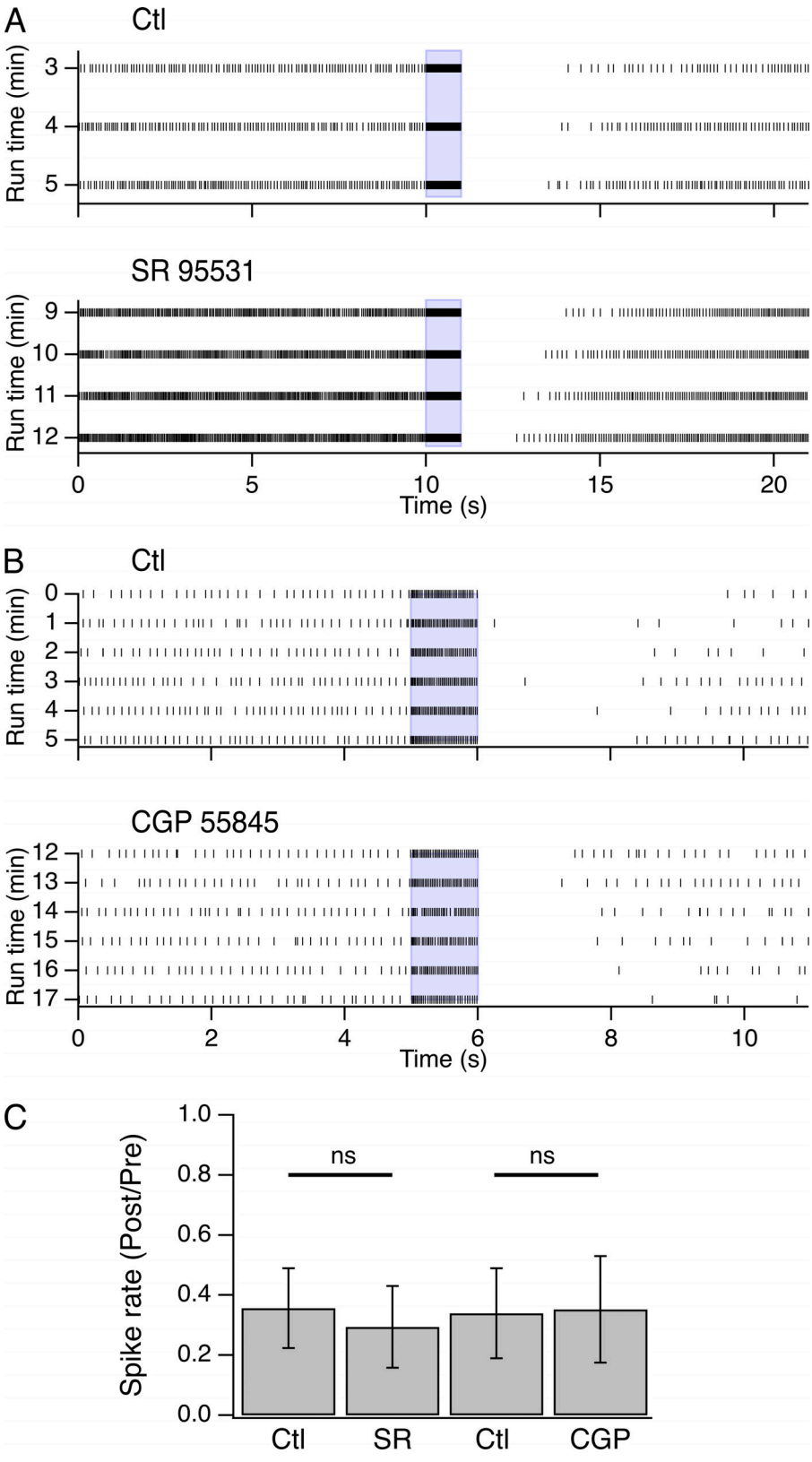

Figure 4. **GABAergic synapses do not contribute to PSS. (A)** Raster plots for the spike activity recorded from an MLI during 1 s optical activation under control conditions (upper panel) and after the addition of 30 µM of the GABA-A R antagonist SR95531 to the bathing solution (lower panel, starting 4 min after the drug was added to the bath). **(B)** Raster plots from a different MLI subject to 1 s optical activation under control conditions (upper panel) and after the addition of 40 µM of the GABA-B R antagonist CGP 55845 to the bathing solution (lower panel, starting 7 min after the drug was added). **(C)** Pooled data on the ratio of the spike rate during the 1 s period after the end of the light pulse over the spike rate preceding the light.

Discussion

Our study shows that optical activation of ChR2 expressed in MLIs in adult mice has a dual effect. It increases MLI firing during light stimulation, but firing decreases below the basal rate following the stimulation. This PSS is not unique to MLIs and has been observed after optogenetic stimulation of ChR2 in PCs in slices (Lee et al., 2015), although it was not reported from work with PCs in vivo (Deverett et al., 2019; Sarnaik and Raman, 2018). Pauses in firing were also found after electrical stimulation of Golgi cells (Vervaeke et al., 2010). The light-induced

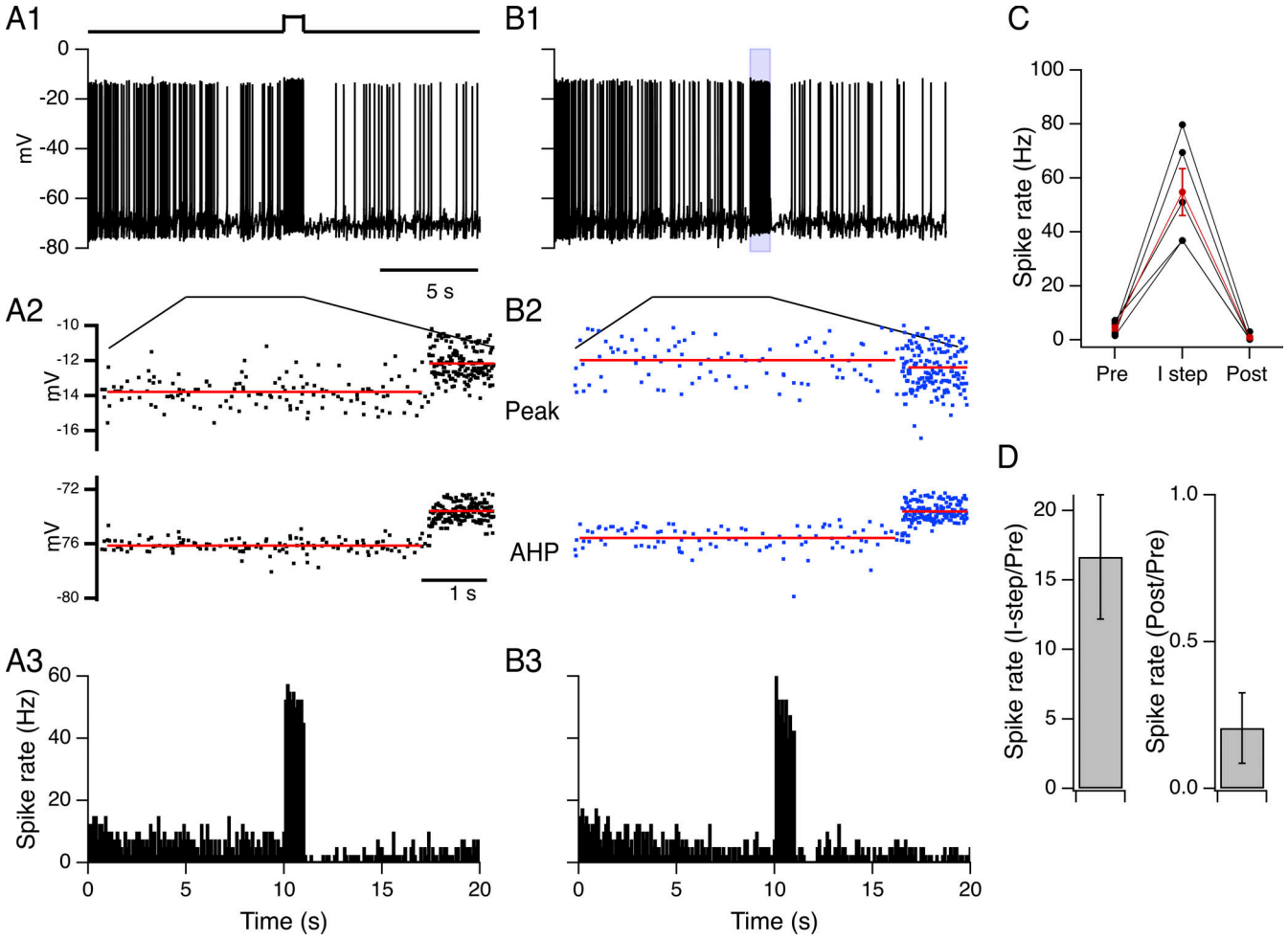

Figure 5. **Individual MLI depolarization mimics the optically induced excitation–inhibition sequence. (A1)** Sample voltage trace from a tight-seal whole cell recording of an MLI maintained in current-clamp configuration. 18 pA steady current was injected to set the basal firing rate at around 6 Hz. A current pulse (25 pA amplitude, 1 s duration; timing indicated in upper trace) increased the firing rate to 50 Hz. The increase was followed by a silent period upon the end of the stimulation. **(A2)** Temporal evolution of the peak spike amplitude (upper trace) and of the minimum of the AHP (bottom trace) starting 5 s before the stimulation and ending with the stimulation. The red lines correspond to the mean values for pre-stimulation (peak: −13.8 mV, AHP: −76.1 mV) and during stimulation (peak: −12.2 mV, AHP: −73.6 mV). **(A3)** PSTH from five repetitions. **(B1)** Voltage recording from the same MLI, in response to a 1 s long optical stimulation. **(B2)** Temporal evolution of peak spike amplitude and AHP minimum, as described in A2. Mean maximum and minimum AP values are shown for pre-stimulation (peak: −12 mV, AHP: −75.6 mV) and during stimulation (peak: −12.4 mV, AHP: −73.7 mV). **(B3)** PSTH from five repetitions. **(C)** Pooled data on spike rates from five MLIs, before the step of current injection (Pre) during the current step (I step) and during the 1 s following the stimulation (Post; cell injected with the same current as in the Pre period). For each MLI, three to seven repetitions were performed. **(D)** Ratios for the increase in spike rate during the current step (left) and for the decrease observed after the current step.

sequence of excitation–inhibition is also noticeable in slice recordings of ChR2 expressing neurons from the brain stem and the thalamic reticular nucleus (Zhao et al., 2011) suggesting that PSS may be widespread. The underlying mechanism, however, has to date not been addressed. Here, we show that the pause in firing does not rely on the interconnected MLI-MLI circuit but rather on a modification of intrinsic MLI excitability properties. This PSS phenomenon differs from the depolarization block reported for other neuronal types in which light pulses lasting 10–100 ms induce an increase in spike rate that is not sustained throughout the pulse duration (Herman et al., 2014). By contrast, in MLIs, the spike rate increase induced by ChR2 photoactivation exhibits minor adaptation during illumination. Only as the light pulse ends does firing stop abruptly. This pause in firing occurs for stimulations lasting 200 ms or 1 s as well as with 50 Hz trains of 10-ms-long pulses lasting 1 s, protocols which are often used to assess effects of optical activation of specific neuronal subtypes during behavior (for recent examples in the cerebellum, see Deverett et al., 2019; Sarnaik and Raman, 2018).

We also find that the temporal pattern of excitation–inhibition can be induced in MLIs with direct electrical stimulation in current-clamp recordings. This result argues against the possibility that optical stimulation could induce PSS through a direct effect on membrane properties that would be unrelated to ChR2 activation. ChR2-gated channels are known to be calcium permeant (Nagel et al., 2003) and are likely to contribute to PSS. Nevertheless, the similarity of the responses elicited by

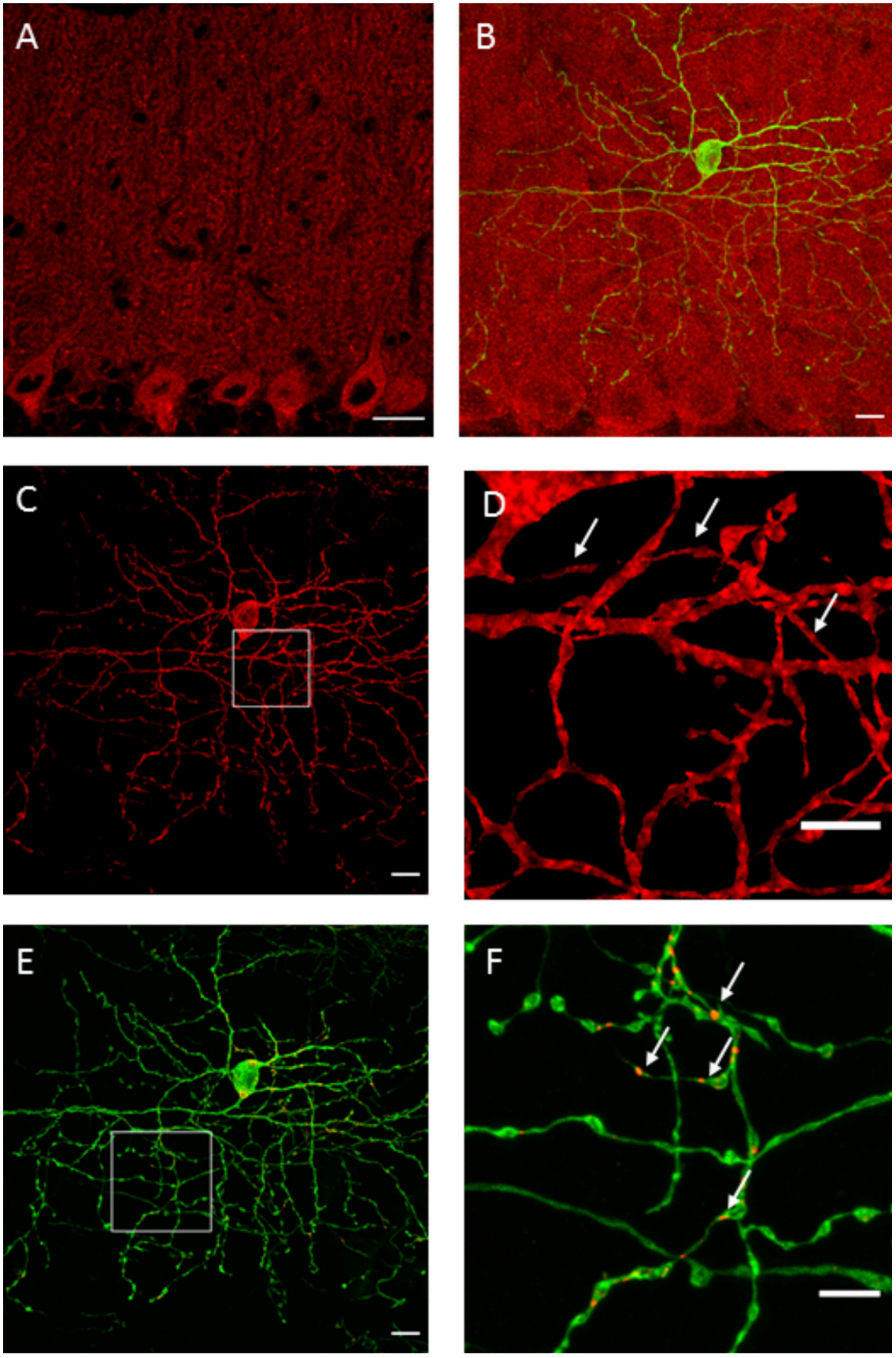

Figure 6. **Expression pattern of KCa1.1 channels in MLIs. (A)** Confocal immunofluorescence image of a sagittal cerebellar slice from a nNOS-ChR2 BAC mouse stained with an antibody targeting Slo1 KCa1.1 channels. The signal is present at the PC soma as well as throughout the molecular layer. **(B–F)** Maximum

intensity projection images (37 planes at 0.4 um interval) from dual GFP/GCaMP3 and Slo1 staining following the ckit:cre sparse GCaMP3 expression strategy. The green channel displays the GFP/GCaMP3 signals while the red channel displays the Slo1 signals. **(B)** Superposition of the two channels. **(C)** Slo1 signal extracted by applying a digital mask from the GFP channel to the Slo1 channel. **(D)** Zoom of the axon initial segment, indicated by white arrows. **(E)** Thresholding applied to the Slo1 signal suggests channel clustering, as indicated by white arrows in F. Calibration bars were 20 µm in A, 10 µm in B, C, and E, and 5 µm in D and F.

electrical and optical means indicates that the increase in firing rate is the primary driver of the excitation–inhibition pattern.

It is important to note that the present work relies on the use of a transgenic line for ChR2 expression. We favored this approach over the more commonly used viral expression strategies because, as discussed by Zhao et al. (2011), it offers stability of ChR2 expression across animals while avoiding potential side effects of viral injections such as protein overexpression and tissue damage at the injection site. However, caution is called for when comparing our results to those from work based on viral-mediated expression since levels of ChR2 may differ considerably.

MLIs are intrinsically active neurons that fire in an irregular manner in the absence of synaptic inputs (Alcami et al., 2012; Häusser and Clark, 1997). Under physiological conditions, repetitive or sustained MLI excitation is elicited by increased firing of either parallel fibers or climbing fibers (Arlt and Häusser, 2020; Chadderton et al., 2004). Our results suggest that in either case, a biphasic excitation–inhibition sequence may follow in MLIs. Consistent with this prediction, climbing fiber activity has

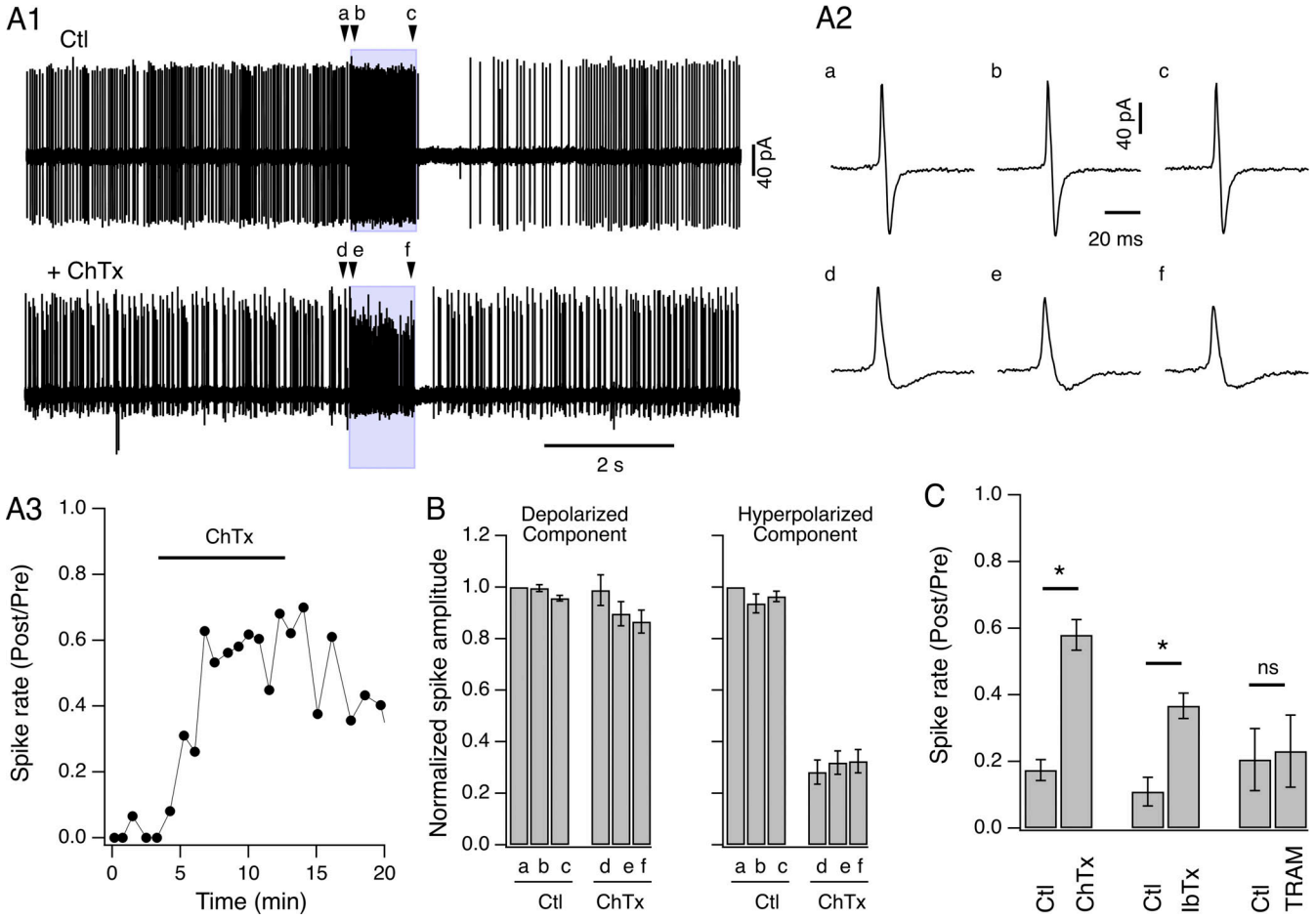

Figure 7. **KCa1.1 channels are involved in PSS. (A1)** Left: Spike activity recorded from an MLI during 1 s optical activation under control condition (upper panel) and 9 min after the addition of 100 nM ChTx (lower panel). **(A2)** Expanded view for average of spikes detected in the last 200 ms preceding optical stimulation (a and d), in the initial 100 ms of photostimulation (b and e) and in the last 100 ms of photostimulation (c and f), as indicated by arrowheads in A1. The 40-pA calibration bar applies to all traces. **(A3)** Time course for the ChTx-induced change in the spike rate ratio for the MLI shown in A1. The optical stimulation protocol was performed at intervals of 0.7–1 min. **(B)** Pooled data from six MLIs on the amplitudes of the depolarized (left) and hyperpolarized (right) components of the spike waveform before optical stimulation (bars a), in the initial 100 ms of the photostimulation (bars b), and in the last 100 ms of the photostimulation (bars c). Data have been normalized to pre-stimulus values in control saline (a). They are shown in control conditions (Ctl; bars a, b, and c) and in the presence of ChTx (bars d, e, and f). **(C)** Pooled data for the effect of ChTx (N = 6; Wilcoxon paired test P = 0.03), IbTx (N = 6; Wilcoxon paired test P = 0.03), and TRAM-34 (N = 5; Wilcoxon paired test P = 0.62) on the light-induced PSS.

recently been shown to elicit such a sequence in a fraction of MLIs (Arlt and Häusser, 2020).

MLI firing influences the electrical activity of neighboring MLIs within a common parasagittal plane through electrical and chemical synapses in a graded manner (Alcami and Marty, 2013; Chavas and Marty, 2003; Häusser and Clark, 1997; Kim et al., 2014; Kim and Augustine, 2020; Mann-Metzer and Yarom, 1999; Rieubland et al., 2014). Therefore, the presence of a PSS after optogenetic stimulation of MLIs is bound to alter the spatio-temporal pattern of activity in the MLI network.

In addition to influencing neighboring MLIs, MLIs regulate the activity of PCs. While a single action potential in a presynaptic MLI can elicit a short pause in a postsynaptic PC (Arlt and Häusser, 2020), bursts of MLI activity have the potential to alter PC firing over long periods of time (Oldfield et al., 2010). With a spontaneously active presynaptic MLI, pauses following bursts are likely to activate PC firing for two reasons. Firstly, as PC firing is tonically inhibited by MLIs (Häusser and Clark, 1997), the absence of firing in the presynaptic MLI during PSS tends to favor firing in the postsynaptic PC. Additionally, because of a strong I_h current in PCs (Oldfield et al., 2010; Williams et al., 2002), the PC hyperpolarization during light stimulation should produce a rebound simple spike facilitation (for review, see De Zeeuw et al., 2011). Thus, following light offset, the persistent activation of I_h combined with cessation of MLI inhibition likely leads to a strong activation of PC firing. By this mechanism, an excitation–inhibition sequence in a presynaptic MLI may translate into an inhibition–excitation sequence in a postsynaptic PC. A similar situation occurs at the next synapse between PCs and principal cells of deep cerebellar nuclei (Aizenman and Linden, 1999; Llinás and Mühlethaler, 1988; Mouginot and Gähwiler, 1995). Overall, MLIs, PCs, and principal neurons of deep cerebellar nuclei form a cascade of cells that are each capable of burst firing and that are linked to each other by inhibitory synapses, raising the possibility of transmissions of bursts and pauses, with sign changes, at each synapse.

Our pharmacological manipulations indicate that the firing pause engages KCa1.1 channels. Although block of these channels significantly decreased the pause, it did not eliminate it, indicating that other channels are likely involved. The results of Fig. 7 further suggest that KCa1.1 channels have two distinct effects on MLI firing: they shorten APs, and they induce pauses after AP bursts. The first effect is favored by the sensitivity of KCa1.1 channels to depolarization (Marty, 1981) and by the close physical association of KCa1.1 channels to voltage-gated calcium channels (e.g., in PCs: Indriati et al., 2013). This effect is rapid and phasic as it follows the time course of individual APs and of the associated local calcium transients. The second effect underlies the pause. It follows much slower kinetics as it reflects the elevation of the global calcium concentration. In ChTx, both effects are blocked, leading both to (1) longer APs, and (2) pause suppression. To explain the long duration of the pause, it is important to consider that MLIs have high concentrations of the calcium binding protein parvalbumin which, because of its slow unbinding rate, slows down the decay of intracellular calcium rises (Collin et al., 2005). The time constant for the slower component of decay for AP-evoked calcium rises in MLI axons is comprised between 1 and 1.5 s (Collin et al., 2005), and it is compatible with the time course of PSS described here. Parvalbumin is expressed in two other classes of GABAergic interneurons of the cerebellar cortex that exhibit PSS (PCs: Lee et al., 2015, and Golgi cells: Vervaeke et al., 2010). Thus, PSS may be a common feature of parvalbumin-containing neurons.

Many interneurons including MLIs have very short spike durations, a feature that likely contributes to allowing for high-frequency firing. Spike shortening in interneurons has often been attributed to specific voltage-activated K^+ channels including Kv3-1 and Kv3-2 (review by Rudy and McBain [2001]; Goldberg et al. [2005]). Cerebellar basket cells contain a high density of Kv3.2 channels in the pinceau region (Bobik et al., 2004) and these channels likely contribute to AP shortening. Furthermore, direct recordings from basket cell axons yield evidence for both Kv3 and Kv1 channels (Southan and Robertson, 2000) and recent work demonstrates spike broadening when Kv1 channels are inhibited or mutated (Begum et al., 2016). The present results suggest that in addition to or in conjunction with channels of the Kv3 and Kv1 families, KCa1.1 channels play a crucial role in the fast repolarization of the membrane potential at the end of each spike.

The immediate cessation of spiking at the end of photostimulation suggests that the increase in cytosolic calcium resulting from repetitive firing induces KCa1.1 channel activation near resting potential values. This would appear paradoxical since neuronal KCa1.1 channels are considered to have very low open probability at resting V_m when calcium is in the low micromolar range (review by Contet et al. [2016]). A potential explanation would involve regulation by accessory subunits of the γ family, which shift the voltage-dependence of KCa1.1 channel opening toward hyperpolarized values, allowing for considerable opening probability at low calcium (Yan and Aldrich, 2012); for review, see Gonzalez-Perez and Lingle, 2019. Evidence that such a mechanism accounts for the activation of KCa1.1 channels in mouse cochlear inner hair cells at negative potentials and in the absence of cytosolic calcium (Thurm et al., 2005) has been provided from studies of mice with deletions of a specific γ subunit (γ2; Lingle et al., 2019). Unfortunately, there is no information at present on the complement of regulatory subunits associated with KCa1.1 channels in cerebellar MLIs. Quantitative PCR from human tissue revealed considerable cerebellar expression for γ4 (Yan and Aldrich, 2012), but as MLIs account for a small part of the total cerebellar PCR results, it remains unclear whether they express any of the γ protein family.

Acknowledgments

Christopher J. Lingle served as editor.

We thank A. Marty for discussions during this work and for comments on the manuscript.

This work was supported by the Agence National de la Recherche (project REWINHIB, ANR-18-CE16-0010-01 to I. Llano) and a doctoral fellowship to M. Kassa. We acknowledge the use of the animal rearing service and the imaging platform of the BioMedTech Facilities (INSERM US36, CNRS UMS2009, Université de Paris).

The authors declare no competing financial interests.

Author contributions: M. Kassa and I. Llano designed, conducted, and analyzed experiments. A. Jalil designed and performed the immunocytochemistry and confocal imaging work. J. Bradley designed the viral construct and sparse labeling strategy. I. Llano wrote the manuscript, and all authors contributed to editing the final version.

Submitted: 26 July 2021
Revised: 6 July 2022
Accepted: 7 October 2022

References

Aizenman, C.D., and D.J. Linden. 1999. Regulation of the rebound depolarization and spontaneous firing patterns of deep nuclear neurons in slices of rat cerebellum. *J. Neurophysiol.* 82:1697–1709. https://doi.org/10.1152/jn.1999.82.4.1697

Alcami, P., R. Franconville, I. Llano, and A. Marty. 2012. Measuring the firing rate of high-resistance neurons with cell-attached recording. *J. Neurosci.* 32:3118–3130. https://doi.org/10.1523/JNEUROSCI.5371-11.2012

Alcami, P, and A. Marty. 2013. Estimating functional connectivity in an electrically coupled interneuron network. *Proc. Natl. Acad. Sci. USA.* 110: E4798–E4807. https://doi.org/10.1073/pnas.1310983110

Arlt, C., and M. Häusser. 2020. Microcircuit rules governing impact of single interneurons on Purkinje cell output in vivo. *Cell Rep.* 30:3020–3035.e3. https://doi.org/10.1016/j.celrep.2020.02.009

Astorga, G., J. Bao, A. Marty, G.J. Augustine, R. Franconville, A. Jalil, J. Bradley, and I. Llano. 2015. An excitatory GABA loop operating in vivo. *Front. Cell. Neurosci.* 9:275. https://doi.org/10.3389/fncel.2015.00275

Astorga, G., D. Li, L. Therreau, M. Kassa, A. Marty, and I. Llano. 2017. Concerted interneuron activity in the cerebellar molecular layer during rhythmic oromotor behaviors. *J. Neurosci.* 37:11455–11468. https://doi.org/10.1523/JNEUROSCI.1091-17.2017

Begum, R., Y. Bakiri, K.E. Volynski, and D.M. Kullmann. 2016. Action potential broadening in a presynaptic channelopathy. *Nat. Commun.* 7: 12102. https://doi.org/10.1038/ncomms12102

Bobik, M., M.H. Ellisman, B. Rudy, and M.E. Martone. 2004. Potassium channel subunit Kv3.2 and the water channel aquaporin-4 are selectively localized to cerebellar pinceau. *Brain Res.* 1026:168–178. https://doi.org/10.1016/j.brainres.2004.07.088

Bock, T., and G.J. Stuart. 2016. The impact of BK channels on cellular excitability depends on their subcellular location. *Front. Cell. Neurosci.* 10: 206. https://doi.org/10.3389/fncel.2016.00206

Candia, S., M.L. Garcia, and R. Latorre. 1992. Mode of action of iberiotoxin, a potent blocker of the large conductance Ca^{2+}-activated K^+ channel. *Biophys. J.* 63:583–590. https://doi.org/10.1016/S0006-3495(92)81630-2

Carta, I., C.H. Chen, A.L. Schott, S. Dorizan, and K. Khodakhah. 2019. Cerebellar modulation of the reward circuitry and social behavior. *Science.* 363:eaav0581. https://doi.org/10.1126/science.aav0581

Chadderton, P., T.W. Margrie, and M. Häusser. 2004. Integration of quanta in cerebellar granule cells during sensory processing. *Nature.* 428: 856–860. https://doi.org/10.1038/nature02442

Chater, T.E., J.M. Henley, J.T. Brown, and A.D. Randall. 2010. Voltage- and temperature-dependent gating of heterologously expressed channelrhodopsin-2. *J. Neurosci. Methods.* 193:7–13. https://doi.org/10.1016/j.jneumeth.2010.07.033

Chavas, J., M.E. Forero, T. Collin, I. Llano, and A. Marty. 2004. Osmotic tension as a possible link between GABA(A) receptor activation and intracellular calcium elevation. *Neuron.* 44:701–713. https://doi.org/10.1016/j.neuron.2004.11.002

Chavas, J., and A. Marty. 2003. Coexistence of excitatory and inhibitory GABA synapses in the cerebellar interneuron network. *J. Neurosci.* 23: 2019–2031. https://doi.org/10.1523/jneurosci.23-06-02019.2003

Collin, T., M. Chat, M.G. Lucas, H. Moreno, P. Racay, B. Schwaller, A. Marty, and I. Llano. 2005. Developmental changes in parvalbumin regulate presynaptic Ca^{2+} signaling. *J. Neurosci.* 25:96–107. https://doi.org/10.1523/JNEUROSCI.3748-04.2005

Contet, C., S.P. Goulding, D.A. Kuljis, and A.L. Barth. 2016. BK channels in the central nervous system. *Int. Rev. Neurobiol.* 128:281–342. https://doi.org/10.1016/bs.irn.2016.04.001

De Zeeuw, C.I., F.E. Hoebeek, L.W.J. Bosman, M. Schonewille, L. Witter, and S.K. Koekkoek. 2011. Spatiotemporal firing patterns in the cerebellum. *Nat. Rev. Neurosci.* 12:327–344. https://doi.org/10.1038/nrn3011

Deverett, B., M. Kislin, D.W. Tank, and S.S.-H. Wang. 2019. Cerebellar disruption impairs working memory during evidence accumulation. *Nat. Commun.* 10:3128. https://doi.org/10.1038/s41467-019-11050-x

Engbers, J.D.T., D. Anderson, H. Asmara, R. Rehak, W.H. Mehaffey, S. Hameed, B.E. McKay, M. Kruskic, G.W. Zamponi, and R.W. Turner. 2012. Intermediate conductance calcium-activated potassium channels modulate summation of parallel fiber input in cerebellar Purkinje cells. *Proc. Natl. Acad. Sci. USA.* 109:2601–2606. https://doi.org/10.1073/pnas.1115024109

Faber, E.S.L., and P. Sah. 2003. Calcium-activated potassium channels: Multiple contributions to neuronal function. *Neuroscientist.* 9:181–194. https://doi.org/10.1177/1073858403009003011

Gao, Z., M. Proietti-Onori, Z. Lin, M.M. Ten Brinke, H.-J. Boele, J.-W. Potters, T.J.H. Ruigrok, F.E. Hoebeek, and C.I. De Zeeuw. 2016. Excitatory cerebellar nucleocortical circuit provides internal amplification during associative conditioning. *Neuron.* 89:645–657. https://doi.org/10.1016/j.neuron.2016.01.008

Goldberg, E.M., S. Watanabe, S.Y. Chang, R.H. Joho, Z.J. Huang, C.S. Leonard, and B. Rudy. 2005. Specific functions of synaptically localized potassium channels in synaptic transmission at the neocortical GABAergic fast-spiking cell synapse. *J. Neurosci.* 25:5230–5235. https://doi.org/10.1523/JNEUROSCI.0722-05.2005

Gomez, L.C., S.-Y. Kawaguchi, T. Collin, A. Jalil, M.D.P. Gomez, E. Nasi, A. Marty, and I. Llano. 2020. Influence of spatially segregated IP3-producing pathways on spike generation and transmitter release in Purkinje cell axons. *Proc. Natl. Acad. Sci. USA.* 117:11097–11108. https://doi.org/10.1073/pnas.2000148117

Gonzalez-Perez, V., and C.J. Lingle. 2019. Regulation of BK channels by beta and gamma subunits. *Annu. Rev. Physiol.* 81:113–137. https://doi.org/10.1146/annurev-physiol-022516-034038

Gu, N., K. Vervaeke, and J.F. Storm. 2007. BK potassium channels facilitate high-frequency firing and cause early spike frequency adaptation in rat CA1 hippocampal pyramidal cells. *J. Physiol.* 580:859–882. https://doi.org/10.1113/jphysiol.2006.126367

Häusser, M., and B.A. Clark. 1997. Tonic synaptic inhibition modulates neuronal output pattern and spatiotemporal synaptic integration. *Neuron.* 19:665–678. https://doi.org/10.1016/s0896-6273(00)80379-7

Heiney, S.A., J. Kim, G.J. Augustine, and J.F. Medina. 2014. Precise control of movement kinematics by optogenetic inhibition of Purkinje cell activity. *J. Neurosci.* 34:2321–2330. https://doi.org/10.1523/JNEUROSCI.4547-13.2014

Herman, A.M., L. Huang, D.K. Murphey, I. Garcia, and B.R. Arenkiel. 2014. Cell type-specific and time-dependent light exposure contribute to silencing in neurons expressing channelrhodopsin-2. *Elife.* 3:e01481. https://doi.org/10.7554/eLife.01481

Hermann, A., and C. Erxleben. 1987. Charybdotoxin selectively blocks small ca-activated K channels in aplysia neurons. *J. Gen. Physiol.* 90:27–47. https://doi.org/10.1085/jgp.90.1.27

Indriati, D.W., N. Kamasawa, K. Matsui, A.L. Meredith, M. Watanabe, and R. Shigemoto. 2013. Quantitative localization of Cav2.1 (P/Q-type) voltage-dependent calcium channels in Purkinje cells: Somatodendritic gradient and distinct somatic coclustering with calcium-activated potassium channels. *J. Neurosci.* 33:3668–3678. https://doi.org/10.1523/JNEUROSCI.2921-12.2013

Kim, J., and G.J. Augustine. 2020. Molecular layer interneurons: Key elements of cerebellar network computation and behavior. *Neuroscience.* 462:22–35. https://doi.org/10.1016/j.neuroscience.2020.10.008

Kim, J., S. Lee, S. Tsuda, X. Zhang, B. Asrican, B. Gloss, G. Feng, and G.J. Augustine. 2014. Optogenetic mapping of cerebellar inhibitory circuitry reveals spatially biased coordination of interneurons via electrical synapses. *Cell Rep.* 7:1601–1613. https://doi.org/10.1016/j.celrep.2014.04.047

Kimpo, R.R., J.M. Rinaldi, C.K. Kim, H.L. Payne, and J.L. Raymond. 2014. Gating of neural error signals during motor learning. *Elife.* 3:e02076. https://doi.org/10.7554/eLife.02076

Lee, K.H., P.J. Mathews, A.M.B. Reeves, K.Y. Choe, S.A. Jami, R.E. Serrano, and T.S. Otis. 2015. Circuit mechanisms underlying motor memory formation in the cerebellum. *Neuron.* 86:529–540. https://doi.org/10.1016/j.neuron.2015.03.010

Lingle, C.J., P.L. Martinez-Espinosa, A. Yang-Hood, L.E. Boero, S. Payne, D. Persic, B. V-Ghaffari, M. Xiao, Y. Zhou, X.-M. Xia, et al. 2019. LRRC52 regulates BK channel function and localization in mouse cochlear inner

hair cells. *Proc. Natl. Acad. Sci. USA*. 116:18397–18403. https://doi.org/10.1073/pnas.1907065116

Llinás, R., and M. Mühlethaler. 1988. Electrophysiology of guinea-pig cerebellar nuclear cells in the in vitro brain stem-cerebellar preparation. *J. Physiol.* 404:241–258. https://doi.org/10.1113/jphysiol.1988.sp017288

Mann-Metzer, P., and Y. Yarom. 1999. Electrotonic coupling interacts with intrinsic properties to generate synchronized activity in cerebellar networks of inhibitory interneurons. *J. Neurosci.* 19:3298–3306. https://doi.org/10.1523/jneurosci.19-09-03298.1999

Marty, A. 1981. Ca-dependent K channels with large unitary conductance in chromaffin cell membranes. *Nature*. 291:497–500. https://doi.org/10.1038/291497a0

Mattis, J., K.M. Tye, E.A. Ferenczi, C. Ramakrishnan, D.J. O'Shea, R. Prakash, L.A. Gunaydin, M. Hyun, L.E. Fenno, V. Gradinaru, et al. 2011. Principles for applying optogenetic tools derived from direct comparative analysis of microbial opsins. *Nat. Methods*. 9:159–172. https://doi.org/10.1038/nmeth.1808

Misonou, H., M. Menegola, L. Buchwalder, E.W. Park, A. Meredith, K.J. Rhodes, R.W. Aldrich, and J.S. Trimmer. 2006. Immunolocalization of the Ca^{2+}-activated K^+ channel Slo1 in axons and nerve terminals of mammalian brain and cultured neurons. *J. Comp. Neurol.* 496:289–302. https://doi.org/10.1002/cne.20931

Mouginot, D., and B.H. Gähwiler. 1995. Characterization of synaptic connections between cortex and deep nuclei of the rat cerebellum in vitro. *Neuroscience*. 64:699–712. https://doi.org/10.1016/0306-4522(94)00456-f

Nagel, G., T. Szellas, W. Huhn, S. Kateriya, N. Adeishvili, P. Berthold, D. Ollig, P. Hegemann, and E. Bamberg. 2003. Channelrhodopsin-2, a directly light-gated cation-selective membrane channel. *Proc. Natl. Acad. Sci. USA*. 100:13940–13945. https://doi.org/10.1073/pnas.1936192100

Nguyen-Vu, T.D.B., R.R. Kimpo, J.M. Rinaldi, A. Kohli, H. Zeng, K. Deisseroth, and J.L. Raymond. 2013. Cerebellar Purkinje cell activity drives motor learning. *Nat. Neurosci.* 16:1734–1736. https://doi.org/10.1038/nn.3576

Niday, Z., and B.P. Bean. 2021. BK channel regulation of after-potentials and burst firing in cerebellar Purkinje neurons. *J. Neurosci.* 41:2854–2869. https://doi.org/10.1523/JNEUROSCI.0192-20.2021

Oldfield, C.S., A. Marty, and B.M. Stell. 2010. Interneurons of the cerebellar cortex toggle Purkinje cells between up and down states. *Proc. Natl. Acad. Sci. USA*. 107:13153–13158. https://doi.org/10.1073/pnas.1002082107

Prestori, F., I. Montagna, E. D'Angelo, and L. Mapelli. 2020. The optogenetic revolution in cerebellar investigations. *Int. J. Mol. Sci.* 21:2494. https://doi.org/10.3390/ijms21072494

Rieubland, S., A. Roth, and M. Häusser. 2014. Structured connectivity in cerebellar inhibitory networks. *Neuron*. 81:913–929. https://doi.org/10.1016/j.neuron.2013.12.029

Rothman, J.S., and R.A. Silver. 2018. NeuroMatic: An integrated open-source software toolkit for acquisition, analysis and simulation of electrophysiological data. *Front. Neuroinf.* 12:14. https://doi.org/10.3389/fninf.2018.00014

Rudy, B., and C.J. McBain. 2001. Kv3 channels: Voltage-gated K^+ channels designed for high-frequency repetitive firing. *Trends Neurosci.* 24:517–526. https://doi.org/10.1016/s0166-2236(00)01892-0

Sarnaik, R., and I.M. Raman. 2018. Control of voluntary and optogenetically perturbed locomotion by spike rate and timing of neurons of the mouse cerebellar nuclei. *Elife*. 7:e29546. https://doi.org/10.7554/eLife.29546

Southan, A.P., and B. Robertson. 2000. Electrophysiological characterization of voltage-gated K^+ currents in cerebellar basket and Purkinje cells: Kv1 and Kv3 channel subfamilies are present in basket cell nerve terminals. *J. Neurosci.* 20:114–122. https://doi.org/10.1523/jneurosci.20-01-00114.2000

Storm, J.F. 1987. Action potential repolarization and a fast after-hyperpolarization in rat hippocampal pyramidal cells. *J. Physiol.* 385:733–759. https://doi.org/10.1113/jphysiol.1987.sp016517

Tan, Y.P., and I. Llano. 1999. Modulation by K^+ channels of action potential-evoked intracellular Ca2+ concentration rises in rat cerebellar basket cell axons. *J. Physiol.* 520:65–78. https://doi.org/10.1111/j.1469-7793.1999.00065.x

Thurm, H., B. Fakler, and D. Oliver. 2005. Ca^{2+}-independent activation of BKCa channels at negative potentials in mammalian inner hair cells. *J. Physiol.* 569:137–151. https://doi.org/10.1113/jphysiol.2005.094680

Trigo, F.F., J.E.T. Corrie, and D. Ogden. 2009. Laser photolysis of caged compounds at 405 nm: Photochemical advantages, localisation, phototoxicity and methods for calibration. *J. Neurosci. Methods*. 180:9–21. https://doi.org/10.1016/j.jneumeth.2009.01.032

Vervaeke, K., A. Lorincz, P. Gleeson, M. Farinella, Z. Nusser, and R.A. Silver. 2010. Rapid desynchronization of an electrically coupled interneuron network with sparse excitatory synaptic input. *Neuron*. 67:435–451. https://doi.org/10.1016/j.neuron.2010.06.028

Villette, V., M. Chavarha, I.K. Dimov, J. Bradley, L. Pradhan, B. Mathieu, S.W. Evans, S. Chamberland, D. Shi, R. Yang, et al. 2019. Ultrafast two-photon imaging of a high-gain voltage indicator in awake behaving mice. *Cell*. 179:1590–1608.e23. https://doi.org/10.1016/j.cell.2019.11.004

Williams, S.R., S.R. Christensen, G.J. Stuart, and M. Häusser. 2002. Membrane potential bistability is controlled by the hyperpolarization-activated current I(H) in rat cerebellar Purkinje neurons in vitro. *J. Physiol.* 539:469–483. https://doi.org/10.1113/jphysiol.2001.013136

Womack, M.D., C. Chevez, and K. Khodakhah. 2004. Calcium-activated potassium channels are selectively coupled to P/Q-type calcium channels in cerebellar Purkinje neurons. *J. Neurosci.* 24:8818–8822. https://doi.org/10.1523/JNEUROSCI.2915-04.2004

Womack, M.D., C. Hoang, and K. Khodakhah. 2009. Large conductance calcium-activated potassium channels affect both spontaneous firing and intracellular calcium concentration in cerebellar Purkinje neurons. *Neuroscience*. 162:989–1000. https://doi.org/10.1016/j.neuroscience.2009.05.016

Yan, J., and R.W. Aldrich. 2012. BK potassium channel modulation by leucine-rich repeat-containing proteins. *Proc. Natl. Acad. Sci. USA*. 109:7917–7922. https://doi.org/10.1073/pnas.1205435109

Zhao, S., J.T. Ting, H.E. Atallah, L. Qiu, J. Tan, B. Gloss, G.J. Augustine, K. Deisseroth, M. Luo, A.M. Graybiel, and G. Feng. 2011. Cell type–specific channelrhodopsin-2 transgenic mice for optogenetic dissection of neural circuitry function. *Nat. Methods*. 8:745–752. https://doi.org/10.1038/nmeth.1668